# Confinement Discerns Swarmers from Planktonic Bacteria

Weijie Chen[1, 2], Neha Mani[1, †], Hamid Karani[1], Hao Li[2], Sridhar Mani[2, *], Jay X. Tang[1, *]

[1] Department of Physics, Brown University, 182 Hope St., Providence, RI 02912, USA

[2] Department of Medicine, Albert Einstein College of Medicine, 1300 Morris Park Ave, Bronx, NY10461, USA

* Corresponding Authors

Email: sridhar.mani@einsteinmed.org; jay_tang@brown.edu

[†] Present address: Hunter College High School, 71 E 94th St, New York, NY 10128, USA

## Author Contribution

W.C., N.M., J.X.T., and S.M. conceived and designed the work. W.C. and N.M. performed the experiments and analyzed the data. H.K. performed the computational simulations. H.L. isolated the bacteria strains and prepared the mouse tissues. W.C., H.K., S.M., and J.X.T. wrote the paper.

## Conflict of interest

Weijie Chen, Neha Mani, Jay X. Tang and Sridhar Mani filed a U.S. patent application (Application No. 63033369). Other authors declare no conflict of interest.

## Acknowledgment

We thank Daniel B. Kearns from Indiana University at Bloomington for providing the *Bacillus subtilis* 3610 bacteria strain, Cori Bargmann at Rockefeller University for gifting us the bacteria strain *Serratia marcescens* Db10. We thank Hui Ma for his assistance in the clean room and discussion of the work. NIH Grant 1R01CA222469-01 supported this work.

## Abstract

Powered by flagella, many species of bacteria exhibit collective motion on a solid surface commonly known as swarming. Physical changes like cell elongation and hyper flagellation have been shown to accompany swarming phenotype. Less noticeable, however, are the contrasts of collective motion between the swarming cells and the planktonic cells of comparable cell density. Here, we show that when confined by microwells of specific sizes mounted on a soft agar surface, novel bacteria *Enterobacter* sp. SM3 under swarming condition exhibited "single-swirl" motion pattern distinct from "multi-swirl" motion pattern formed by its concentrated planktonic counterpart. We hypothesize that "rafting behavior" of the swarming bacteria upon dilution might account for the motion pattern difference. This was further validated through computational simulation where swarming cells are modeled by lower repulsion and stronger alignment among them than planktonic cells. Our new technical approach also enabled us to observe swarming on a non-agar tissue surface.

## Introduction

Motility is an essential characteristic for bacteria. Although energy-consuming, it provides high returns, enabling cells to uptake nutrients efficiently and escape from noxious environments[1]. In a host environment, bacterial motility is also an essential phenotype that intimately relates to virulence through complex regulatory networks[2]. Swimming and swarming are two common motility phenotypes mediated by flagella. Whereas planktonic phenotype defines the motility of individual bacteria, a collective movement powered by rotating flagella[3] on a partially solidified surface defines swarming[4]. In swarming, bacteria utilize their flagella to navigate, two-dimensionally, through a medium and acquire necessary molecules for the maintenance of homeostasis and overall survival[5]. Morphological changes like cell elongation may or may not occur in all swarming bacteria[6]. Thus, concentrated swimming bacteria are often called "a swarm of bacteria" without requiring precise identification of swarming motility, per se. Nevertheless, microbiologists believe that swarming and swimming are fundamentally different motility types. For instance, studies found that compared with swimming cells, the requirement for flagella torque is higher for swarming *B. subtilis*[7]; swarming *E. coli* remodel their chemotaxis pathway[8]; and in swarming *P. aeruginosa*, the production of virulence factors and antibiotic resistance increases[9]. A recent study has demonstrated a medically relevant distinction between swarming and swimming: a particular strain of swarming endobacteria protect against mice intestinal inflammation while their swimming counterparts could not[10]. The evidence to date that shows swarming is different from swimming comes mostly from biological data. However, precise biophysical visualization and quantitation of these differences are lacking. In this report, using *Enterobacter* sp. SM3, a novel bacteria strain that possesses both swimming and swarming motilities, we show distinct biophysical characteristics between these two types of motility under confined, circular geometry of a particular range of sizes.

Studies have shown that geometric constraints have profound influence on patterns of microswimmers' collective motion. For example, these constraints may create mesoscopic or macroscopic coherent structures such as swirls and jets[11-13]. Circular confinement, in particular, could stabilize a suspension of motile bacteria into a spiral vortex[14-16]. Here, we compare the behaviors of bacteria in swarming and planktonic states under quasi-2D circular confinement. Many species of bacteria show distinctive motion patterns while confined. This characteristic may

lead to future diagnostic applications since there are growing associations between bacterial swarming and virulence pathologies.

## Results

### Swarming *Enterobacter* Sp. SM3 forms large single swirls up to 100 μm diameter

A novel bacterial strain *Enterobacter* Sp. SM3 (NCBI BioProject PRJNA558971), isolated in 2014 from DSS induced clitic mice, has been previously studied for motility[17] and infectivity[10]. SM3 is a strong swarmer, expanding rapidly on 0.5% agar with collective motion of multilayers of cells at the edge. We mounted a PDMS chip containing circular microwells on the agar so that bacteria in confinement could rotate for more than 3 hours (details with illustration in Methods). Under confinement in circular wells in the diameter range of 31-90 μm, swarming SM3 shows single swirls. In contrast, SM3 planktonic cells concentrated from the liquid medium form mesoscale vortices (multiple swirls) in the same size range, with the exception of the smallest well diameter of 31 μm. A clear difference is shown at the well diameter of 74 μm (Fig. 1A-D, Movie S1 & S2). This striking difference persists in several well depths, except that the concentrated cells yields small but non-zero vortex order parameter (VOP, defined as illustrated in Fig. 1E) in deeper wells, as opposed to nearly zero VOP in shallow wells (Fig. 1F).

The confinement well diameter has strong influence on the motion pattern in the wells. In smaller wells like 31 μm, even concentrated planktonic SM3 forms a single vortex (Fig. 2A) whereas in larger wells, such as ones of 112 μm diameter, swarming SM3 also breaks into mesoscale vortices (Fig. 2B). The phase diagram shows a single swirl in small confinement for both types. The patterns diverge as confinement size increases, but they converge towards multiple swirls as confinement size reaches 144 μm and larger (Fig. 2C). To further compare the dynamics of the confined swarming and swimming SM3, spatial correlation of the velocity field was calculated for d = 90 μm where the motion patterns differ for swarming and swimming SM3 and for d = 500 μm where both motilities show mesoscale vortices (see method). We computed the correlation function for the inscribed square within a well, which shows the extent to which the velocity at an arbitrary location correlated with the velocity at a distance of $\Delta r$ away from that location. In 90 μm wells, swarming SM3 velocity correlates positively or negatively throughout the whole well (negative values have resulted from the opposite sides of a single swirl). In contrast, swimming

velocity of planktonic cells of comparable concentration does not correlate anymore as Δr went up beyond 25 μm (Fig. 2D). However, in a large open space where both swarming and swimming SM3 break into small vortices, the correlation functions look similar. The characteristic length as the curve first crosses $C_r(\Delta r) = 0$, which also represents the size of the mesoscale vortices, of planktonic SM3 is 27 μm and 33 μm for swarming SM3 (Fig. 2E).

We also tested other bacteria such as *Enterobacter* Sp. SM1, *Serratia marcescens* (including one lab strain Db10 and another strain H3 isolated from a human patient), *Citrobacter koseri* (H6), and *Bacillus subtilis* 3610. All the tested strains showed similar motion pattern divergence between confined planktonic cells and swarming cells like SM3 with the exception of *B. subtilis* (Fig. S1A, see discussion).

**The large single swirl behavior is indicative of cohesive cell-cell interaction**

We performed several experiments to explore the cause for the divergence of motion patterns in confinement. First, we rule out cell density difference as the reason for the difference in the confined motion patterns by concentrating planktonic cells to comparable density to that of a naturally expanding swarm on agar (see methods) before mounting the PDMS chip. Second, we noticed that SM3 tends to get elongated when they swarm. We hypothesize that elongated bacteria may enhance the local alignment of the rod-shaped cells and increase the size of vortices in mesoscale turbulence[18]. Thus, we treated SM3 planktonic cells with Cephalexin (CEP) which has been shown to elongate *E. coli* [19] . This treatment indeed caused the cell length to reach that of swarming cells on average (Fig. 3A). However, we found no significant change following centrifugation and CEP treatment of the planktonic SM3 (Fig. 3B). Although CEP treated planktonic SM3 has similar cell length, cell density, and cell speed as that of swarming SM3, we could not restore the single swirl pattern in 74 μm confinement wells (Fig. 3C). Third, noticing a surfactant rim on the swarming SM3 colony edge, we conjectured that surfactants secreted by swarming SM3 might help align the swarmers in confinement. Surfactin was added in several concentrations to planktonic SM3 in order to test whether it could promote a single swirl pattern. However, it did not establish a stable single swirl. Last but not least, we found that adding lyophilized swarming supernatant to swimming SM3 also did not help increase the VOP (Fig. 3C).

Unable to make the concentrated planktonic SM3 form a single swirl in the 74 μm well, we tackled the problem from another angle, by altering the conditions of swarming SM3 in order to break the single swirls. Initially, we tried to physically "damage" the swarming colony by rubbing the swarming colony gently with a piece of PDMS offcut. This operation did not break the single swirl pattern in the wells (Fig. 3D). Then, 0.2% D-mannose was added to the swarming colony to de-cluster bacteria bundles due to cells' sticking to each other. However, this treatment could not alter the single swirl pattern, either (Fig. 3D). Finally, we diluted the swarming cells in LB by 20-fold. After re-concentrating the cells by centrifugation and removing extra LB to recover the initial cell density, these "swarming" SM3 cells were pipetted back on the agar plate. After this treatment, the previous single swirl turned to multiple swirls under the confinement (Fig. 3D), suggesting that these cells now behave much like planktonic cells. We conclude that the single swirl pattern depends on cohesive cell-cell interaction mediated by biochemical factor/s removable by matrix dilution.

**Diluted swarming SM3 show unique dynamic clustering patterns**

We suspected that specific interactions between the neighboring swarming cells were weakened or even diminished upon dilution with the Luria broth (LB) medium. A fifty (50) μL water droplet was applied to the swarming and the concentrated planktonic SM3 colony edges to investigate the potential alignment among the cells at a microscopic scale within the bacterial colony. In the diluted swarming colony, groups of cells formed bacterial rafts, a characteristic feature previously associated with gliding motility[3,20]. Those cells within a polar cluster moving in the same direction in a cohesive pack at the same speed (Movie S3). In contrast, upon dilution of the concentrated planktonic SM3, the cells disperse uniformly, and their moving directions appear random (Movie S4). Swarming SM3 cells tend to move together near the agar surface, while planktonic SM3 cells swim freely in the bulk fluid (Fig. 4A-B). We used the MATLAB PIV toolkit to track the moving bacteria in the image sequences of diluted swarming and planktonic SM3 for comparison. We found that swarming SM3 formed clusters with more than 20 cells on average, while we did not see such clusters of planktonic SM3 cells (Fig. 4C-D). The lingering clusters of cells in the swarming phase upon dilution point to stronger cell-cell cohesive interaction than between planktonic cells.

## Numerical simulation reveals cell-cell interaction to be the key player

To further verify that rafting in swarming is a crucially relevant factor to the motion pattern discrepancy, we performed computer simulations using the Zonal Model where the interactions among the moving particles (short-range repulsion, velocity alignment, and anti-alignment) are considered, all as functions of the particle-particle distance[21,22]. The speed of the particles is fixed for simplicity, but the initial particle positions and initial moving directions are randomized. In the simulations, we interpret the rafting as a lower repulsion force and stronger alignment among the swarmers (see methods and SI methods). We simulated the situation of confined swarmers and planktonic cells in different sizes of circular confinement, as in the experiments. The simulation results mirror the experiment results well: both swarmers and planktonic cells start with single swirl pattern; as the circle size is increased, the planktonic cells break into multi-swirl motion pattern earlier than the swarmers and finally both converge to multi-swirl region (Fig. 5A, compared with Fig. 2C, also see Fig. S2 and Movie S7). We then performed the "dilution" simulation for both states, finding that swarming cells form dynamic clusters when the cell density is above $\rho = 235$ whereas the planktonic cells form a "gas" phase without clustering at all densities (Fig. 5B, Movie S8). This result echoes the experimental results in Fig. 4A. Thus, by encoding stronger cell-cell interaction among the swarming cells, we recovered the experimental results in both confinement and dilution experiments.

## Identifying SM3 motility type on mice mucosal surface

The difference in confined motion patterns enables us to detect bacterial swarming on surfaces other than agar, including physiological environments such as on a mucosal surface. We are unaware of any previous studies or examples regarding bacterial swarming on non-agar surfaces, likely due to technical challenges in dealing with uneven or non-controlled surfaces. The mouse intestinal tissue, for instance, is more than 1 mm thick and non-transparent. Since light cannot penetrate the tissue, observing bacteria directly on the tissue surface is not feasible. Staining or fluorescence labeling may alter the bacterial swarming motility (e.g. SM3 becomes non-swarming once GFP labeled. Unpublished observation). If labeled biochemically, the fluorescence signal weakens when the cells reproduce (e.g., there will be progressively less cell wall labeling of SM3 with Alexa Fluor 488 when cells divide). Using fluorescent beads coated PDMS chips mounted

on SM3 inoculated C57BL6 mouse intestine tissue, we were able to detect swarming motility based on the swirling motion of the beads. This experiment on the mouse intestine tissue confirms that bacterial swarming indeed occurs on a non-agar, physiologically relevant surface (Fig. S3; Movie S5&6, also see SI method).

## Discussion

Mounting PDMS chip on a soft agar plate, we have shown the motion pattern differences between confined planktonic and swarming *Enterobacter* sp. SM3 in the size range of 40 μm ≤ d ≤ 90 μm. Compared with previous work, our experimental setup has the advantage of ensuring stable and sustainable patterns. First, PDMS material does not harm living bacteria cells and is permeable to oxygen[23], which prevents suffocation. Second, we mounted the microchip on a soft agar containing over 97% water, which, via permeability and capillary flow, automatically fills the wells. Finally, the LB agar also provides the necessary nutrients to fuel the bacterial movement in the wells. Therefore, bacterial cells confined in the microwells remain motile for hours, much longer than in droplets surrounded by mineral oil[14,19] or in microfluidic chambers with glass surfaces[11,16], where bacteria movement typically lasted no more than 10 minutes.

Prior studies have proposed different models to explain the circularly confined motion of rod-shaped swimmers[15,19,24]. However, these theories cannot explain the motion pattern difference we observed for confined swarming and planktonic SM3. Noticing that swarming SM3 washed in LB lost the single swirl pattern, we hypothesize that other than cell length or cell speed, the strong cell-cell interaction may be a key factor responsible for the persistence of single swirls in the wells. The mechanism of the rafting phenomenon of swarming cells has not been fully deciphered yet[3]. It might be due to cohesive interaction among neighboring cells together with hydrodynamic effects among 2D-confined peritrichously flagellated bacteria[25]. The cell-cell interaction may further result from biochemical change of cell envelope during swarming (e.g., more long sidechain lipopolysaccharides) or secretions[26]. Once these surrounding matrix or polymers are washed away by ~ 100-fold dilution, the cohesive interactions are diminished, resulting in no dynamic clusters in the dilution experiment and multi-swirl motion pattern under confinement. Reproducing the experimental results via computer simulation, we confirm that the lower repulsion and higher alignment are the key factors, which differentiate swarmers and planktonic cells. Future

work is called upon to explore further the swarmer rafting phenomenon and to investigate on the molecular level which category of substances are mainly responsible for the cell-cell cohesive interaction among the swarming cells.

A spectrum of swarming bacteria has the same characteristic as SM3 (Fig. S1A). These bacteria tested, including SM1, H6, H3, and Db10, all behave like SM3. They all show clustering or cohesive cell-cell interaction when the swarming colony was diluted and uniformly dispersed when the concentrated planktonic cells were diluted. One notable exception is *Bacillus subtilis.* Swarming and concentrated planktonic *Bacillus subtilis* 3610 show the same motion pattern across different confinement sizes. For well diameter $d \leq 90$ μm, both swarming and swimming *B. subtilis* form single swirls while for well diameter $d \geq 112$ μm, they both break into mesoscale vortices. *B. subtilis* is Gram-positive bacteria different from SM3, SM1, H6, H3, and Db10 and we speculate that swarming *B. subtilis* does not have as strong cell-cell interaction as SM3. The interaction is not so different between the swarming and planktonic cells since we found the diluted swarming *B. subtilis* 3610 to disperse uniformly, much like diluted planktonic *B. subtilis* 3610, with no clustering behavior. The swarming colony thickness might also be a key factor for *B. subtilis* to be an outlier here. It is known that swarming *B. subtilis* produces abundant surfactant, resulting in a wide-spread, monolayer, non-compact colony[20,27]. In contrast, swarming SM3 and the other tested bacteria are multilayer colonies that can be as thick as 20 - 40 μm, which may enhance the spatial cell-cell alignment that is much stronger than that among the planktonic cells (Fig. S1B).

Our observation on SM3 confirms the prediction made by Beppu *et al.* that single vortex occurs when the confinement diameter d is smaller than a critical length $l^*$[16]. Here, the critical length for swarming SM3 is ~ 49 μm, whereas, for concentrated planktonic SM3, it is ~ 17 μm. Interestingly, the same bacteria strain in different motility states has two distinct critical lengths. Thus, we were able to use this property to identify the motility types on mouse mucosal surfaces. The beads motion is not a perfect swirl in every well on the colitic tissue because the mucosal surface is not as smooth as the agar surface. There are sags and crests on the inflamed mucosal surface due to the disrupted mucin layer. We conjectured that this unevenness would hinder the swirl formation to a certain extent and intact swirl patterns can be spotted only on limited locations where the mucosal surface is relatively flat. Nevertheless, capturing only a few wells where beads show single swirl motion suffices to show that swarming can happen on the mucosal surface.

Evidence of genetic up/down regulations[28-31] and cell morphology changes (e.g., cell elongation and hyper-flagellation) indicates that swarming is a different phenotype from swimming. Lacking comparison under the same conditions of experiments, one might suspect that bacterial swarming might just be a dense group of cells swimming on a surface[3]. Here, through geometry confinement, we show *Enterobacter* sp. SM3 as an example that swarming manifests different biophysical characteristics from swimming. The key experimental method used in this study differentiates swarming motility from swimming motility and provides a straightforward assay to detect swarming behavior on a given surface visually. The findings of this study provide the rationale for developing applications such as isolating bacterial swarmers from a polymicrobial environment and developing diagnostics for the presence of *in vivo* swarming. A quantitative ranking system for different swarmers could potentially be established based on characteristic well size that stabilizes the confined motion pattern into a single swirl. Such a ranking system will be significant for future investigations on the implications of swarming bacteria on host health and diseases.

## Methods

**PDMS confinement sheet fabrication.** Polydimethylsiloxane (PDMS) microwell confinement sheets with different combinations of well sizes and depths were fabricated using the technique of soft photolithography. Patterns of the confinement were first designed using the software "L-Edit" and then uploaded into a maskless aligner (MLA 150, Heidelberg). On a 3.5-inch silicon wafer (University Wafer Inc.), photoresist gel SQ25 (KemLab, Inc.) was spin-coated at 2,000 rpm (spin speed varies according to the desired coating thickness). After baking, UV exposure, and chemical development, the microwells' designed pattern was shown on the wafer (moulding). Then, PDMS (Dow Corning Sylgard 184) base elastomer was mixed with the curing agent at the ratio of 10:1 in weight. The mixture was cast onto the patterned silicon wafer. Two grams of the mixture ended up with a PDMS sheet about 0.5 mm thick. The PDMS solidified at room temperature within 48 hours and it was cut into pieces and peeled off from the silicon wafer before use (demoulding).

**Bacterial growth and confinement (Fig. 6A).** *Enterobacter* sp. SM3 is a novel swarming bacterial strain isolated from inflammatory mice[10]. SM3 was transferred from - 80°C glycerol stock to fresh LB (Lysogeny Broth: water solution with 10 g/L tryptone, 5 g/L yeast, and 5 g/L NaCl) and shaken overnight (~ 16 h) in a 37°C incubator at 200 rpm. For swarming under confinement

assay (Fig. 6A, red arrows), 2 μL overnight bacterial culture was inoculated on the center of a LB agar plate (10 g/L tryptone, 5 g/L yeast, 5 g/L NaCl, and 5 g/L Agar; volume = 20 mL/plate) and kept in a 37℃ incubator. After 2.5 h of swarming, a PDMS chip (~ 1 $cm^2$) was mounted upon the edge of the swarming colony and the Petri dish was transferred onto the microscope stage for observation. For swimming under confinement assay (Fig. 6A, blue arrows), overnight bacterial culture was resuspended in fresh LB (1:100 in volume) and shaken in the 37℃ incubator at 200 rpm for 2.5 h. The freshly grown culture was centrifuged at 1,500 g for 10 min and ~ 98.6% of the supernatant was removed so that the resultant cell density is about 70 times the fresh grown culture. Ten (10) μL concentrated bacteria culture was inoculated on the LB agar plate, and PDMS chip was mounted immediately. The plate was then transferred onto the microscope stage for observation. For other strains of bacteria, including *Bacillus Subtilis* 3610, the procedure was the same as that of SM3. On one PDMS chip, there are thousands of wells and when mounted on a bacteria spot or colony edge, hundreds of them are occupied by bacteria. The PDMS chip was first brought to contact with the bacteria and then gently mounted onto the agar. In this case, there was a cell density gradient across an array of wells, with the wells closer to the bacteria spot or colony center having relatively higher cell density. In the experiment, we focused on the area where the confined bacteria showed collective motion, i.e. the cell density was not too high to jam the well or too low so that each cell was moving independently.

**Bacterial cell density measurement (Fig. 6B).** 2.5 h freshly grown SM3 was subjected to different factors of dilution in LB, such as $10^2$, $10^3$, until $10^8$. 50 μL of each diluted culture was inoculated and spread on 1.5 % LB agar plate (10 g/L tryptone, 5 g/L yeast, 5 g/L NaCl, and 15 g/L Agar; volume = 20 mL/plate) and was incubated at 37℃ for 16 h. Bacterial colonies appeared on the agar plates and the number of colonies was counted for the dilution that resulted in the colony's number on the order of 100. The colony forming unit per microliter (CFU/mL) was calculated by dividing the colony number by the sampled volume. For swarming SM3, the cell density was measured in a similar way. On the edge of the swarming colony, a chunk of swarming SM3 (~ 1 mm wide) was picked by an eight (8) mm-wide square spatulate containing a small piece of agar on the bottom to ensure all the cells in that region were sampled. The 1 mm x 8 mm chunk of swarming SM3 was then mixed into 1 mL LB for CFU determination. The colony thickness was assumed to be uniform across the sample and was measured by microscopy focusing on the top of the colony and the top of the agar surface (i.e., at the bottom of the colony), keeping track

of the readings on the fine adjustment knob. Particles of baby powder (~ several micrometers in diameter) were spread on the surfaces of the swarm colony and the agar to aid in the microscope focus. The thickness of the swarming colony was calculated based on the calibration of the knob turning tick readings. Then the cell density was estimated by CFU/mL. CFU was calculated for both swarming and swimming SM3 to make sure the cell densities of these two cases were comparable inside the wells. We consider colony forming unit counting a better way to control the live cell number than simply using the volume fraction because: 1, Dead cells that count in the volume fraction will not contribute to the motion in the well, but they will be excluded in CFU calculation; 2, It is technically difficult to measure the volume of dense bacterial suspension using pipetting method due to high viscosity.

**Bacterial cell length and motility.** For swimming SM3, 2.5 h freshly grown culture was diluted 100 times in LB and 50 μL of which was transferred on a glass slide and covered with a coverslip. The sample slide was placed under the microscope (Olympus CKX41, 20X) and image sequences were captured. Cell lengths were measured using ImageJ (v1.59e) freehand label tool. Cell speed was calculated by traveling trajectory length divided by the traveling duration (~ 1s). For swarming SM3, a chunk of swarming bacteria was collected from the edge of the swarming colony and mixed with 1 mL LB. A droplet of 50 μL mixed culture was sandwiched by a glass slide and a cover slip, and the rest of the procedure was the same as that for the swimming SM3.

**Swimming SM3 with different treatments. i), Cephalexin treatment.** Overnight SM3 culture was diluted 100 times in fresh LB and incubated in a 37℃ shaker at 200 rpm for 1.5 h. Cephalexin (CEP) was added to the culture so that the resultant concentration of CEP was 60 μg/mL. The culture was kept in the shaker for another two (2) h before use. **ii), Surfactin additions.** After 2.5 h regrown culture was centrifuged, more supernatant was removed than usual, and surfactin was added so that the resulting concentrations of surfactin were 10, 50, 100, 500 μM while the cell density remained comparable to that of swarming SM3. **iii), Addition of swarming supernatant.** Before swarming SM3 covered the plate, the colony was scratched carefully using a piece of PDMS (~ 0.5 $cm^2$) and transferred into 1 mL deionized water. The mixture was sucked into a syringe and filtered with a 0.2 μm filter. Then the solution was lyophilized to powder and then dissolved into the concentrated swimming SM3 of roughly the same volume as the collected

swarm fluid. Thus, the concentration of the swarming supernatant was kept the same after being transferred to swimming SM3.

**Swarming SM3 with different treatments. i), Rubbed with PDMS.** After SM3 swarmed on the agar plate for 2.5 h, a piece of PDMS (~ 0.5 $cm^2$) was used to rub gently on the edge of the swarming colony so that the swarming cells were disturbed. A PDMS confinement chip was then mounted on the disturbed region for observation. **ii)**, **Spun down in LB.** After swarming for 2.5 h, SM3 cells were collected from the edge of the colony using the blotting method[32]. The cells were blotted by a piece of spare PDMS and transferred to 1 mL LB. The swarming cells were centrifuged at 1,500g, and LB was removed in order to restore the initially high cell density. Ten (10) μL of the swarming cells thus treated were inoculated on a new swarm agar and a PDMS confinement chip was mounted for observation. **iii), Added D-mannose.** A droplet of 50 μL 0.2% (w/v) D-mannose was pipetted on a swarming SM3 colony edge. After 1-2 minutes, when the cell density became uniform again, a piece of PDMS confinement chip was applied to the D-mannose treated region for observation under the microscope.

**VOP measurement and spatial autocorrelation function.** Image sequences of swarming or swimming SM3 under confinement were taken by a microscope camera (ThorLabs, Kiralux CS505MU) and then processed using a particle image velocimetry (PIV) package in MATLAB. The velocity field was marked for the confined bacteria and the VOP was calculated using the equation in Fig. 1E. Using the velocity field information, the spatial autocorrelation function was calculated through the equation $C_r(\Delta r) = < \frac{\boldsymbol{v}(r_0)\cdot\boldsymbol{v}(r_0+\Delta r)}{|\boldsymbol{v}(r_0)^2|} >$, where $r_0$ is the local position vector and $\Delta r$ is the displacement vector[33]. A Python script was written to calculate all the $C_r$ values in the region of interest (ROI) with a label of $\Delta r$ values. These $C_r$ values were then plotted as a function of $\Delta r$.

**Clustering analysis.** On the swarming SM3 colony edge or concentrated swimming SM3 inoculation, a droplet of 50 μL deionized water was added via a pipette. Once the fluid flow stabilizes, image sequences were captured at the locations of the diluted swarming or swimming SM3 samples. In a region of 130 μm x 130 μm, using the PIV toolkit, the velocity field was calculated and the vectors with magnitude below four (4) μm/s were removed. The purpose of the vector validation was to exclude non-motile bacteria. Once the moving cells were identified, a

Python script was implemented to perform the clustering analysis using the function of DBSCAN[34] where the parameter ε was set to 50, which specifies how close points should be to each other to be considered a part of a cluster, and the minimum number of points to form a cluster was set to 20.

**Numerical Simulations.** The numerical simulation consists of a 2D system of $N$ particles. The position **r** of each particle is modeled via the following overdamped Langevin equation:

$$\partial_t \boldsymbol{r_i} = v_0 \widehat{p_i} - \sum_{j \neq i} G_\theta(d_{ex}, r_{ji}) + \sqrt{2D_T}\xi_i \quad (1)$$

It is assumed that particles are cruising at a constant speed of $v_0$ in the direction of $\widehat{p_i} = [\cos(\theta_i), \sin(\theta_i)]$. The second term includes the exclusion forcing term from all neighboring particles residing at a distance $r_{ji}$ closer than the exclusion range $d_{ex}$. The last term is the thermal fluctuation term with the translational diffusivity of $D_T$ and a zero-mean and delta-correlated noise term $\xi$. The direction of motion $\theta_i$ of each particle is updated by the interaction terms $F_\theta$ which includes alignment, anti-alignment and repulsion effects with all neighboring particles and also the rotational diffusion term with diffusivity of $D_r$ and noise term $\zeta$:

$$\partial_t \theta_i = \sum_{j \neq i} F_\theta(\boldsymbol{r_{ji}}, \widehat{p_i}, \widehat{p_j}) + \sqrt{2D_r}\zeta_i \quad (2)$$

The details of the binary interaction terms $G_\theta$ and $F_\theta$ are provided in the Supplementary Material. The simulation starts with random initial position and orientations, followed by numerical integration of equations (1) and (2) using a first-order Euler method. The integration time step $\Delta t$ is chosen small enough to ensure numerical stability and also independence of long-term dynamics from the time step increment. The interaction of particles with circular bounded domain is modeled through a reflective boundary condition, where the particles are reflected off the boundary with an angle equal to their incident angle. In all diluted cases, reflecting solid boundary is replaced with a periodic boundary condition to ensure that boundary scattering is not affecting the dynamics in the bulk.

380 **Figure 1**

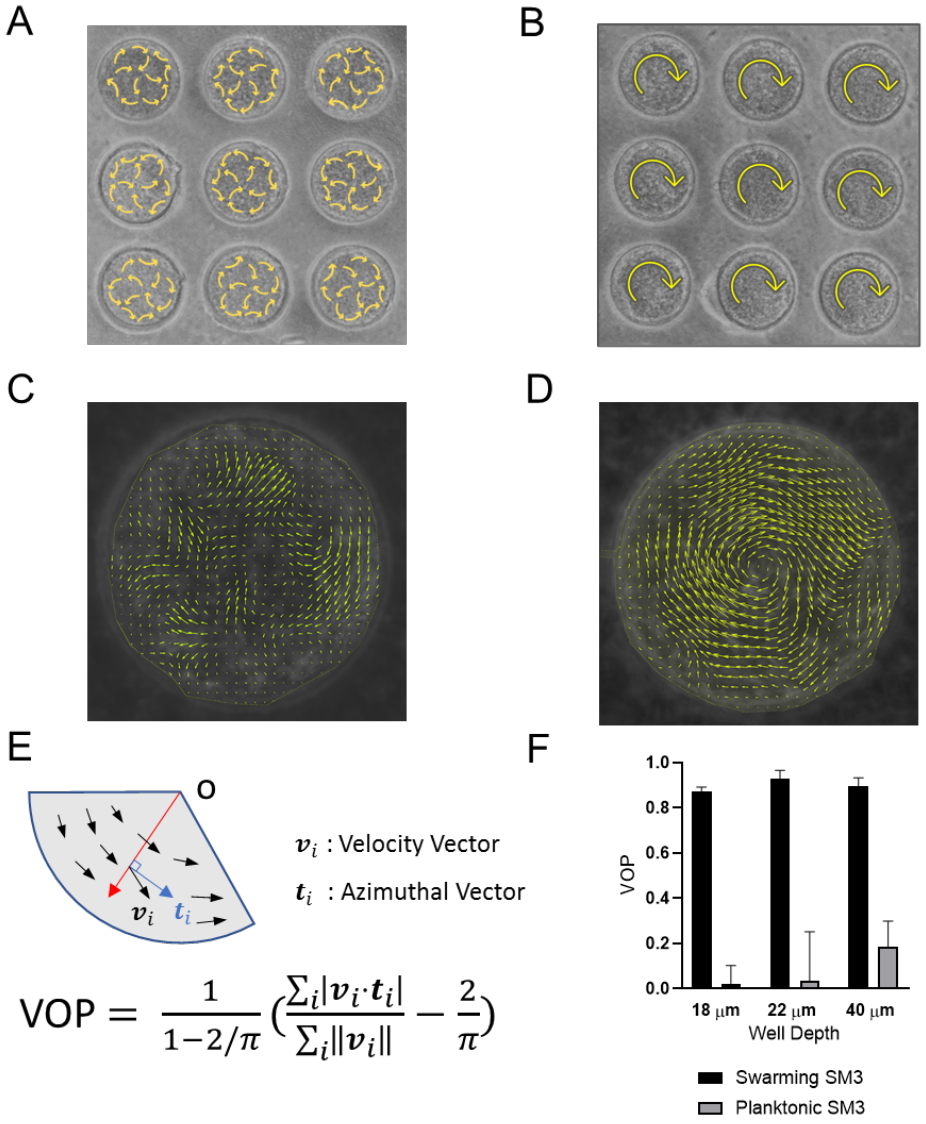


381

382 **Figure 1 | Swirls of *Enterobacter* sp. SM3 under circular confinement.** (A-B) Motion pattern of
383 concentrated planktonic (A) and swarming (B) SM3 in the PDMS microwells of 74 μm in diameter. Circular
384 arrows indicate the direction of bacterial collective motion. (C-D) Velocity field of concentrated planktonic
385 (C) and swarming (D) SM3 in a single microwell. (E) Illustration of how vortex order parameter (VOP) is
386 defined. $|\cdot|$ denotes the absolute value while $\|\cdot\|$ denotes the Euclidean norm. (F) VOP of swarming and
387 swimming SM3 in 74 μm microwells of different depths. The sample size n = 5 for each group and data are
388 represented as mean and standard deviation (+SD).

**Figure 2**

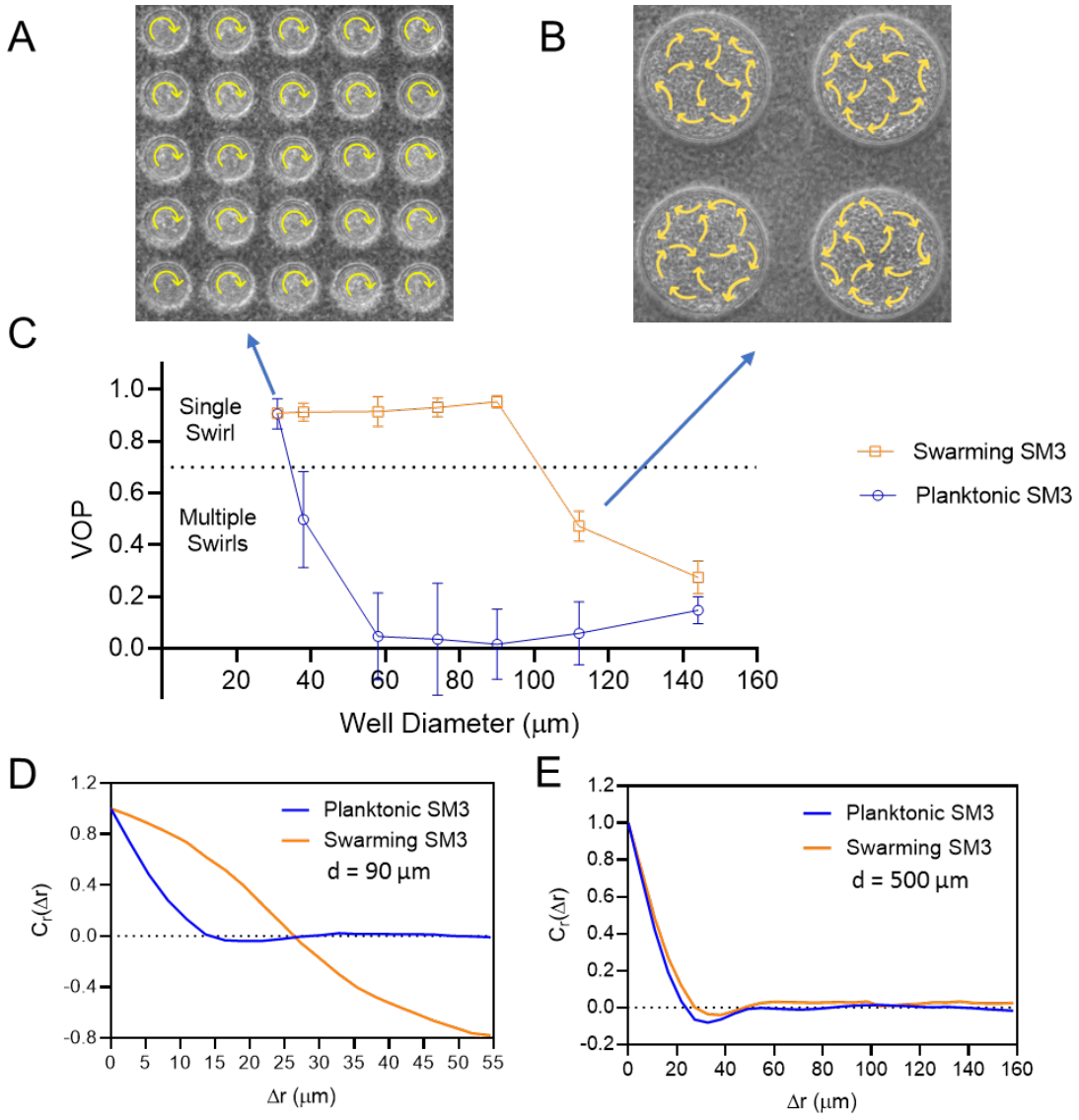


**Figure 2 | The effect of well diameter on confined *Enterobacter* Sp. SM3 motility patterns.** (A-B) Motion pattern of concentrated planktonic SM3 confined in 31 μm (A) and swarming SM3 confined in 112 μm (B) diameter microwells. (C) VOP of swarming and concentrated planktonic SM3 as a function of well diameter. The error bars represent the standard deviations (± SD) for each data point, and the sample size is n = 5. (D-E) Spatial autocorrelations of the bacterial velocity field in the well diameter of 90 μm (D) and 500 μm (E). Unless otherwise noted, the depth of the wells is 22 μm.

**Figure 3**

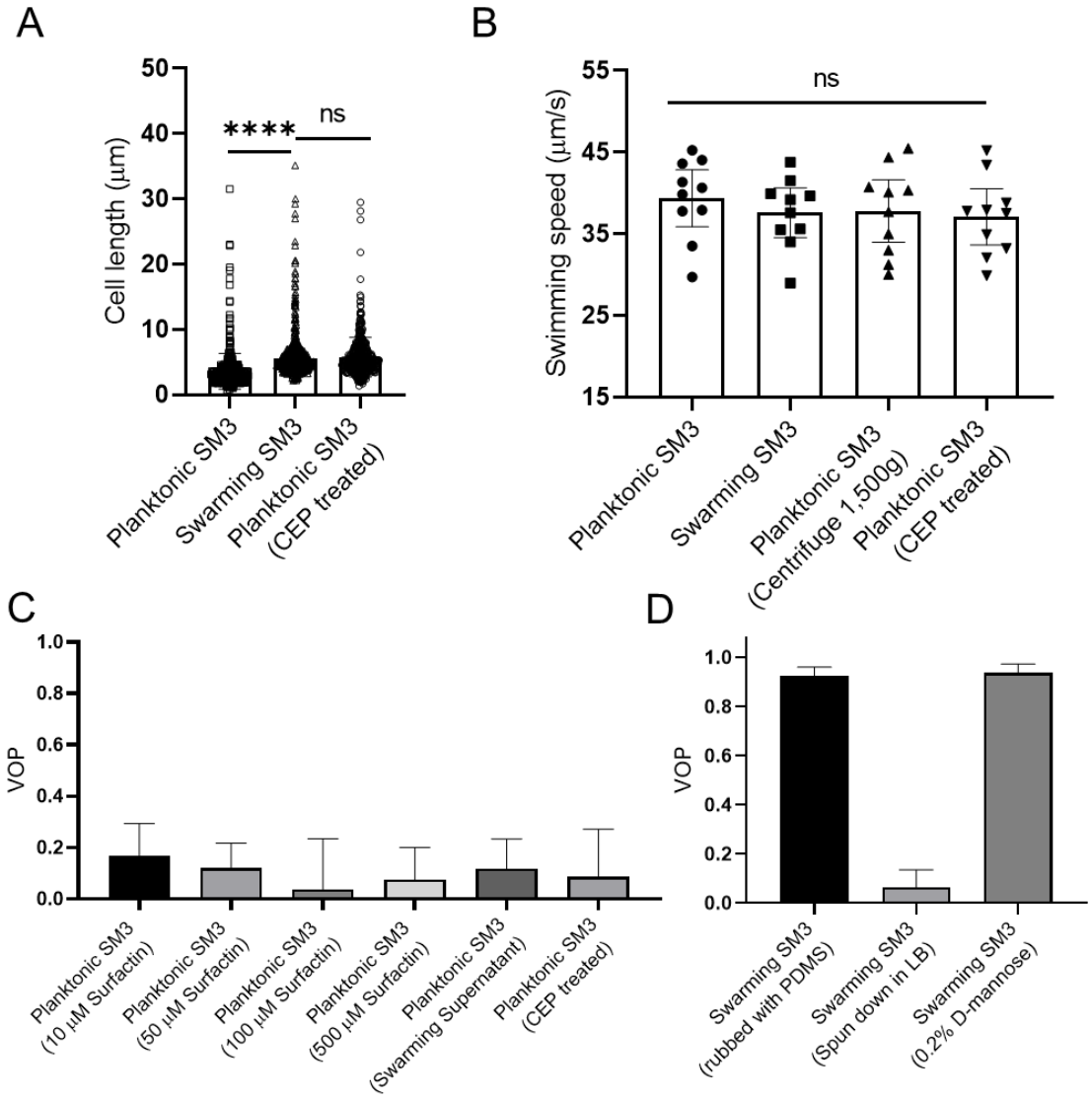


**Figure 3 | Factors that possibly influence the bacterial motion pattern in the well.** (A) Bacterial cell length of planktonic, swarming, and Cephalexin (CEP) treated planktonic SM3, n = 500 for each group. Data are represented as median and interquartile range. **** indicates $P < 0.0001$. ns indicates not significant (Kruskal-Wallis test). (B) Bacterial cell speed of swimming, swarming, centrifuged, and CEP treated swimming SM3, n = 10 for each group. ns, not significant, one-way ANOVA followed by Tukey's post hoc test. (C) VOP of swimming SM3 under 74 μm diameter confinement with different treatments, n = 5 for each group. (D) VOP of swarming SM3 under 74 μm diameter confinement with different treatments, n = 5 for each group. B-D, Data are represented as mean and standard deviation (+SD).

408 **Figure 4**

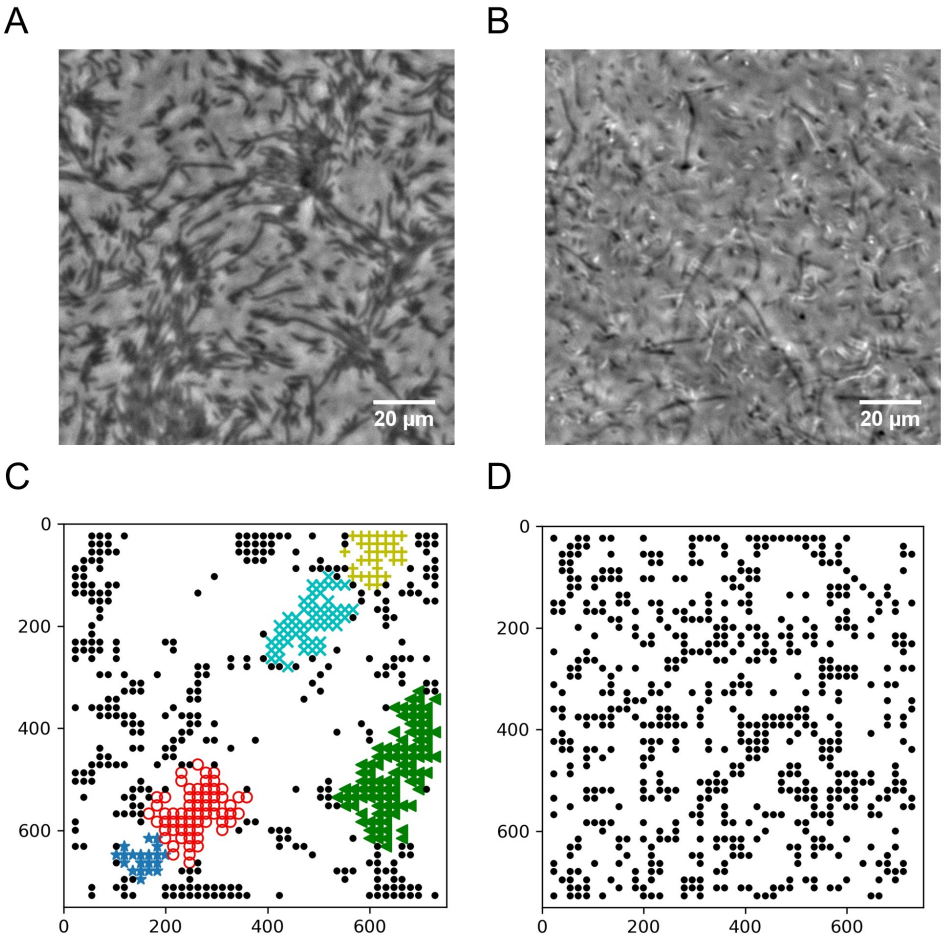


409

410 **Figure 4 | Spatial distribution of swarming and swimming SM3 cells.** (A-B) Snapshots showing diluted
411 swarming SM3 (A) and swimming SM3 (B) on a soft agar surface, respectively. (C-D) DBSCAN clustering
412 analysis of diluted swarming SM3 (C) and swimming SM3 (D). Black dots represent moving bacterial cells
413 and colored markers show cells in clusters, as determined by the program. The axis represents the dimension
414 of the image in pixels.

415 **Figure 5**

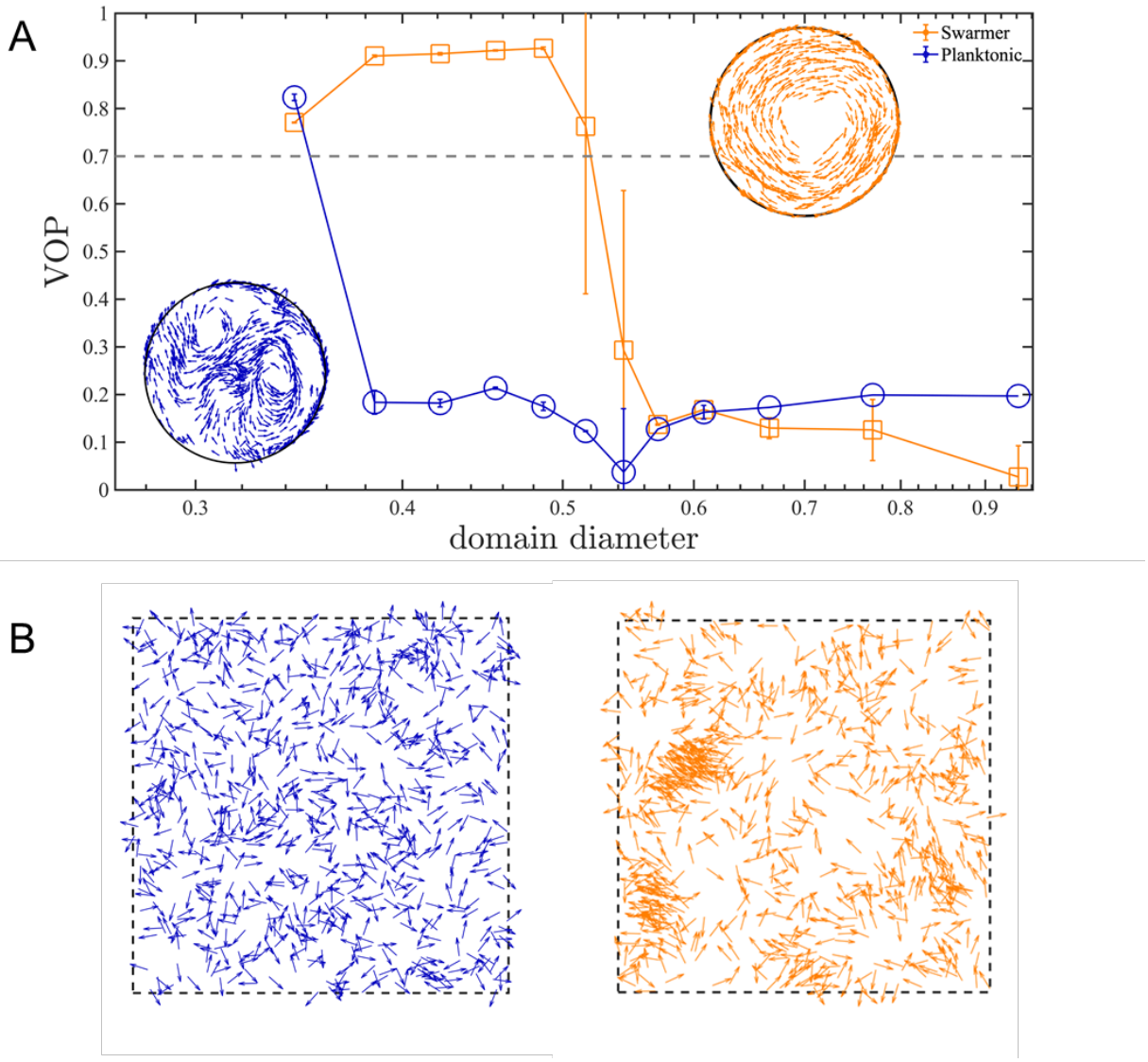


416

417 **Figure 5 | Numerical simulations of planktonic and swarimng SM3 in confinement and open space.**
418 (A) VOP of swarming and concentrated planktonic SM3 as a function of well diameter. The error bars
419 represent the standard deviations (± SD) for each data point, and the sample size is n = 5. The circles on the
420 upper right corner and the lower left corner show representative motion patterns of swarmers and
421 concentrated planktonic cells in the confinement size between 0.38 and 0.5. (B) Planktonic cells (left) and
422 diluted swarming cells (right) with same cell density in a space of periodic boundary condition.

423

424 **Figure 6**

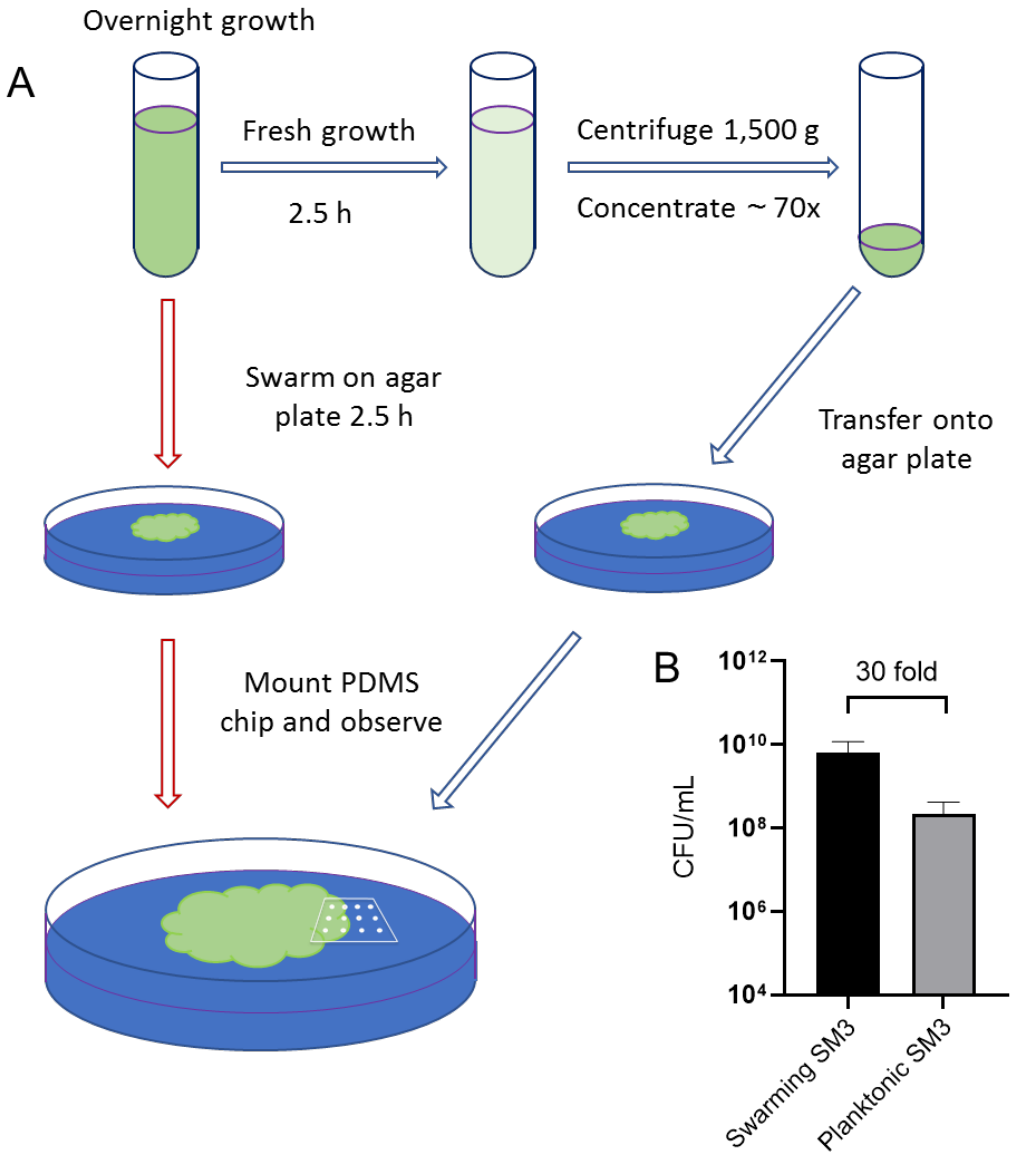


425

426 **Figure 6 | Illustration of experimental procedure.** (A) Schematic of sample preparation procedure. Red
427 arrows represent the assay procedure for swarming bacteria. Blue arrows represent the assay procedure for
428 swimming planktonic bacteria. (B) Cell density measured by colony forming unit (CFU/mL) of swarming
429 SM3 and swimming SM3. Swarming SM3 cell density is measured after SM3 swarming on an agar surface
430 for 2.5 h while swimming SM3 cell density is measured for overnight SM3 culture being regrown in fresh
431 Lysogeny Broth (LB) for 2.5 h. Since cell density of swarming SM3 was higher than that of planktonic
432 SM3, the latter was concentrated before being applied on the agar plate to acquire comparable cell density.

## References


1 Webre, D. J., Wolanin, P. M. & Stock, J. B. Bacterial chemotaxis. *Curr Biol* **13**, R47-R49, doi:Doi 10.1016/S0960-9822(02)01424-0 (2003).

2 Josenhans, C. & Suerbaum, S. The role of motility as a virulence factor in bacteria. *Int J Med Microbiol* **291**, 605-614, doi:Doi 10.1078/1438-4221-00173 (2002).

3 Kearns, D. B. A field guide to bacterial swarming motility. *Nat Rev Microbiol* **8**, 634-644, doi:10.1038/nrmicro2405 (2010).

4 Partridge, J. D. & Harshey, R. M. Swarming: Flexible Roaming Plans. *J Bacteriol* **195**, 909-918, doi:10.1128/Jb.02063-12 (2013).

5 Darnton, N. C., Turner, L., Rojevsky, S. & Berg, H. C. Dynamics of Bacterial Swarming. *Biophys J* **98**, 2082-2090, doi:10.1016/j.bpj.2010.01.053 (2010).

6 Michaels, B. & Tisa, L. S. Swarming motility by Photorhabdus temperata is influenced by environmental conditions and uses the same flagella as that used in swimming motility. *Can J Microbiol* **57**, 196-203, doi:10.1139/W10-119 (2011).

7 Hall, A. N., Subramanian, S., Oshiro, R. T., Canzoneri, A. K. & Kearns, D. B. SwrD (YlzI) Promotes Swarming in Bacillus subtilis by Increasing Power to Flagellar Motors. *J Bacteriol* **200**, doi:UNSP e0052910.1128/JB.00529-17 (2018).

8 Partridge, J. D., Nhu, N. T. Q., Dufour, Y. S. & Harshey, R. M. Escherichia coli Remodels the Chemotaxis Pathway for Swarming. *Mbio* **10**, doi:ARTN e00316-1910.1128/mBio.00316-19 (2019).

9 Overhage, J., Bains, M., Brazas, M. D. & Hancock, R. E. W. Swarming of Pseudomonas aeruginosa is a complex adaptation leading to increased production of virulence factors and antibiotic resistance. *J Bacteriol* **190**, 2671-2679, doi:10.1128/Jb.01659-07 (2008).

10 Chen, W. *et al. Bacterial Swarmers exhibit a Protective Response to Intestinal Stress*, <https://www.biorxiv.org/content/10.1101/759886v3> (2020).

11 Wioland, H., Lushi, E. & Goldstein, R. E. Directed collective motion of bacteria under channel confinement. *New J Phys* **18**, doi:Artn 07500210.1088/1367-2630/18/7/075002 (2016).

12 Wioland, H., Woodhouse, F. G., Dunkel, J. & Goldstein, R. E. Ferromagnetic and antiferromagnetic order in bacterial vortex lattices. *Nat Phys* **12**, 341-U177, doi:10.1038/Nphys3607 (2016).

13 Theillard, M., Alonso-Matilla, R. & Saintillan, D. Geometric control of active collective motion. *Soft Matter* **13**, 363-375, doi:10.1039/c6sm01955b (2017).

14 Wioland, H., Woodhouse, F. G., Dunkel, J., Kessler, J. O. & Goldstein, R. E. Confinement Stabilizes a Bacterial Suspension into a Spiral Vortex. *Phys Rev Lett* **110**, doi:ARTN 26810210.1103/PhysRevLett.110.268102 (2013).

15 Lushi, E., Wioland, H. & Goldstein, R. E. Fluid flows created by swimming bacteria drive self-organization in confined suspensions. *P Natl Acad Sci USA* **111**, 9733-9738, doi:10.1073/pnas.1405698111 (2014).

16 Beppu, K. *et al.* Geometry-driven collective ordering of bacterial vortices. *Soft Matter* **13**, 5038-5043, doi:10.1039/c7sm00999b (2017).

17 Araujo, G., Chen, W. J., Mani, S. & Tang, J. X. Orbiting of Flagellated Bacteria within a Thin Fluid Film around Micrometer-Sized Particles. *Biophys J* **117**, 346-354, doi:10.1016/j.bpj.2019.06.005 (2019).

18 Doostmohammadi, A., Adamer, M. F., Thampi, S. P. & Yeomans, J. M. Stabilization of active matter by flow-vortex lattices and defect ordering. *Nat Commun* **7**, doi:ARTN 1055710.1038/ncomms10557 (2016).

19 Hamby, A. E., Vig, D. K., Safonova, S. & Wolgemuth, C. W. Swimming bacteria power microspin cycles. *Sci Adv* **4**, doi:ARTN eaau012510.1126/sciadv.aau0125 (2018).

20 Be'er, A. & Ariel, G. A statistical physics view of swarming bacteria. *Mov Ecol* **7**, doi:ARTN 910.1186/s40462-019-0153-9 (2019).

21 Grossmann, R., Romanczuk, P., Bar, M. & Schimansky-Geier, L. Pattern formation in active particle systems due to competing alignment interactions. *The European Physical Journal*, 1325-1347, doi:10.1140/epjst/e2015-02462-3 (2015).

22 Grossmann, R., Romanczuk, P., Bar, M. & Schimansky-Geier, L. Vortex arrays and mesoscale turbulence of self-propelled particles. *Phys Rev Lett* **113**, 258104, doi:10.1103/PhysRevLett.113.258104 (2014).

23 Turner, L., Zhang, R. J., Darnton, N. C. & Berg, H. C. Visualization of Flagella during Bacterial Swarming. *J Bacteriol* **192**, 3259-3267, doi:10.1128/Jb.00083-10 (2010).

24 Tsang, A. C. H. & Kanso, E. Circularly confined microswimmers exhibit multiple global patterns. *Phys Rev E* **91**, doi:ARTN 04300810.1103/PhysRevE.91.043008 (2015).

25 Li, Y., Zhai, H., Sanchez, S., Kearns, D. B. & Wu, Y. L. Noncontact Cohesive Swimming of Bacteria in Two-Dimensional Liquid Films. *Phys Rev Lett* **119**, doi:ARTN 01810110.1103/PhysRevLett.119.018101 (2017).

26 Judith P. Armitage, D. G. S., R. J. Rowbury. Alternation in the cell envolope composition of *Proteus Mirabilis* during the development of swarmer cells. *Biochimica et Biophisica Acta* **584**, 389-397 (1979).

27 Jeckel, H. *et al.* Learning the space-time phase diagram of bacterial swarm expansion. *P Natl Acad Sci USA* **116**, 1489-1494, doi:10.1073/pnas.1811722116 (2019).

28 Tremblay, J. & Deziel, E. Gene expression in Pseudomonas aeruginosa swarming motility. *Bmc Genomics* **11**, doi:Artn 58710.1186/1471-2164-11-587 (2010).

29 Wang, Q. F., Frye, J. G., McClelland, M. & Harshey, R. M. Gene expression patterns during swarming in Salmonella typhimurium: genes specific to surface growth and putative new motility and pathogenicity genes. *Mol Microbiol* **52**, 169-187, doi:10.1111/j.1365-2958.2003.03977.x (2004).

30 Morgenstein, R. M., Szostek, B. & Rather, P. N. Regulation of gene expression during swarmer cell differentiation in Proteus mirabilis. *Fems Microbiol Rev* **34**, 753-763, doi:10.1111/j.1574-6976.2010.00229.x (2010).

31 Daniels, R., Vanderleyden, J. & Michiels, J. Quorum sensing and swarming migration in bacteria. *Fems Microbiol Rev* **28**, 261-289, doi:10.1016/j.femsre.2003.09.004 (2004).

32 Darnton, N., Turner, L., Breuer, K. & Berg, H. C. Moving fluid with bacterial carpets. *Biophys J* **86**, 1863-1870, doi:Doi 10.1016/S0006-3495(04)74253-8 (2004).

33 Patteson, A. E., Gopinath, A. & Arratia, P. E. The propagation of active-passive interfaces in bacterial swarms. *Nat Commun* **9**, doi:ARTN 537310.1038/s41467-018-07781-y (2018).

34 Ester, M. K., H. Sander, J. Xu, X. in *Proceedings of the Second International Conference on Knowledge Discovery and Data Mining.* 226-231 (AAAI Press).

519 **Supplementary Information**

520 **Figure S1**

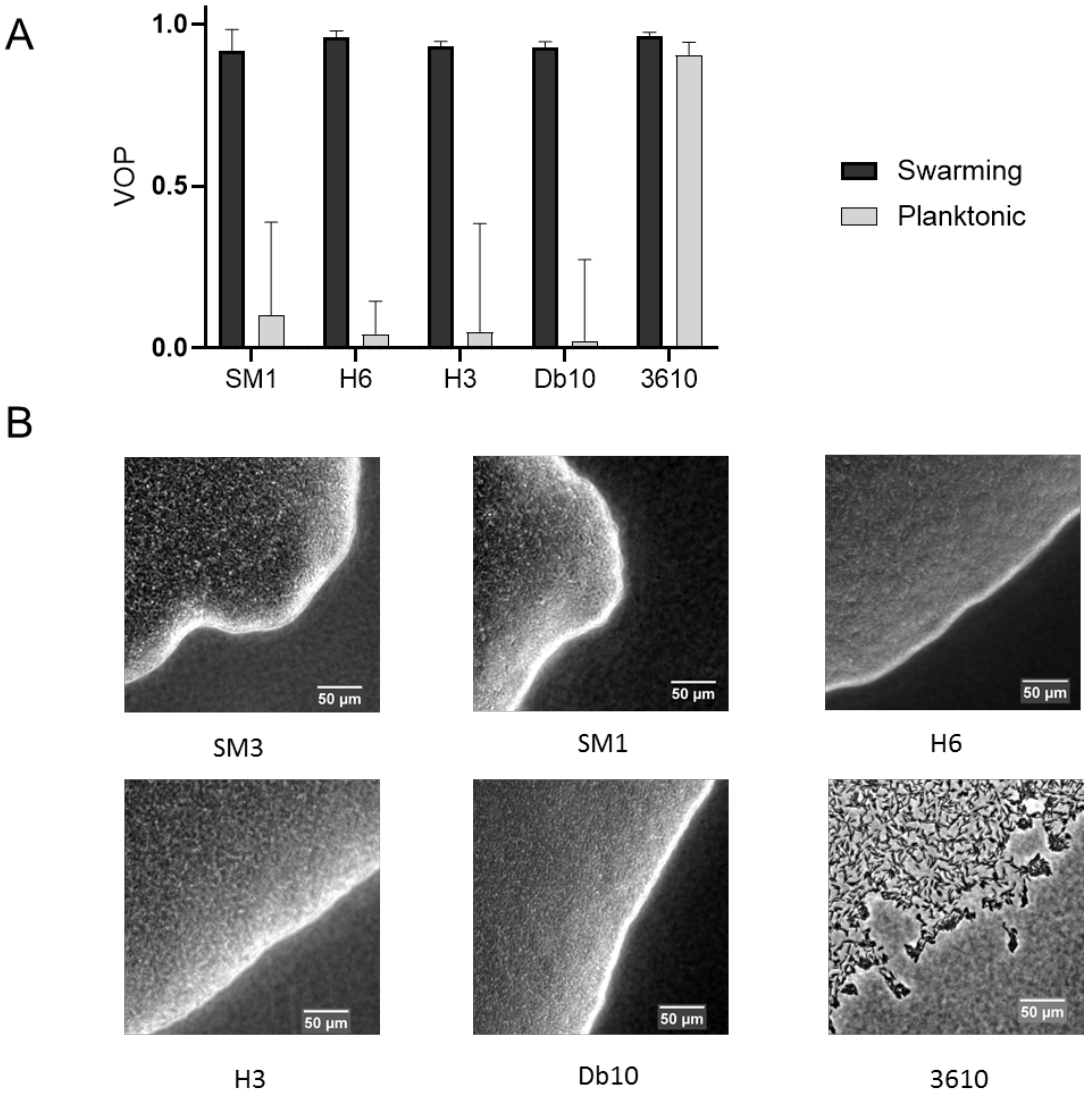


521

522

523 **Figure S1 | Other bacteria under confinement and their swarm front.** (A) VOP of concentrated
524 planktonic and swarming Enterobacter sp. SM1, *Citrobacter koseri* (H6), *Serratia marcescens* (H3),
525 *Serratia marcescens* (Db10) and *Bacillus subtilis 3610* confined in the PDMS microwells of 58 µm in
526 diameter. The bars indicate averages with standard deviation (+SD) over 5 microwells. (B) Swarm front of
527 the tested bacteria. *B. subtilis* 3610 shows monolayer, loose swarming colony while all the other bacteria
528 strains show multilayer, compact swarming colony.

529 **Figure S2**

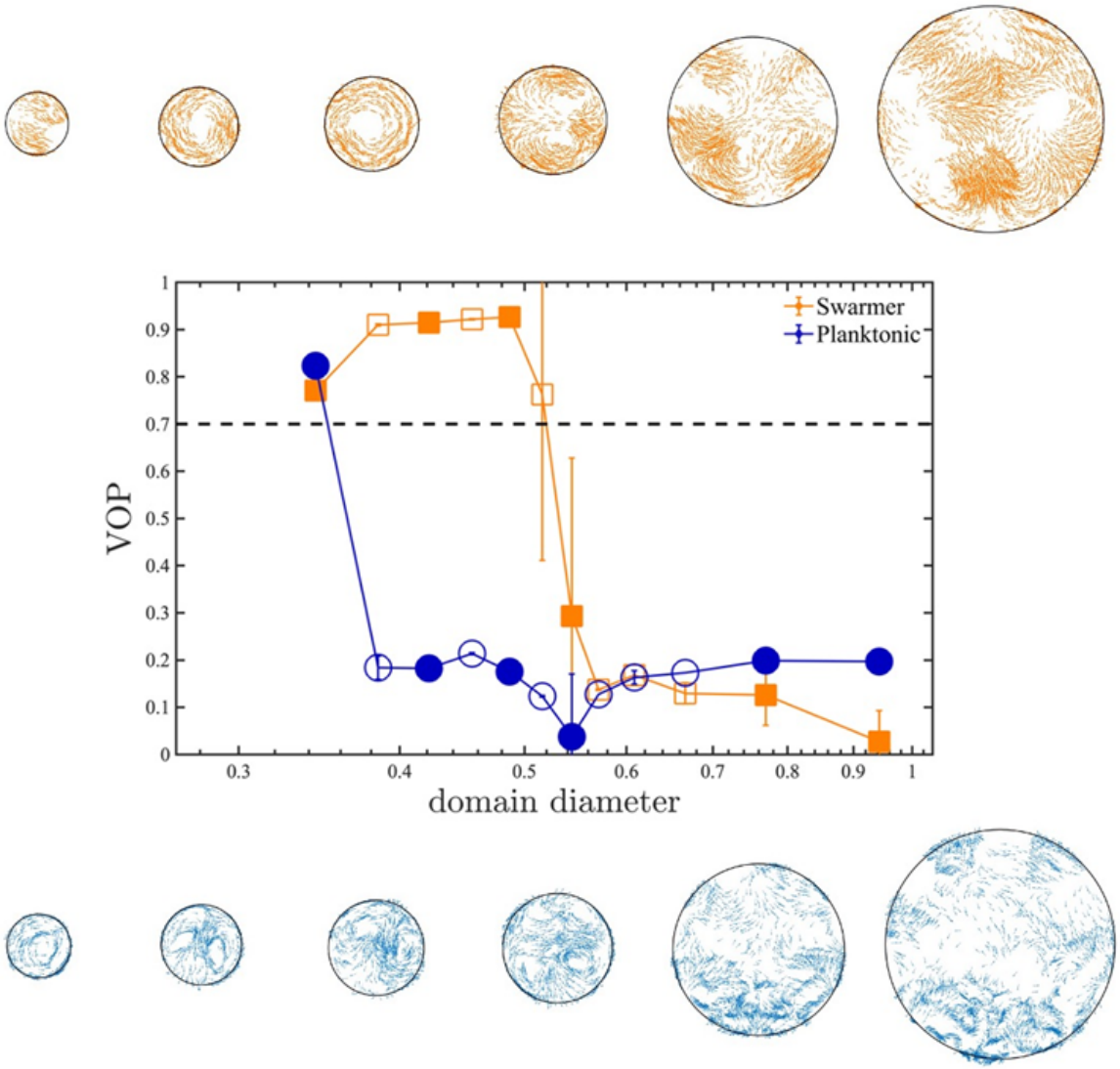


530

531 **Figure S2 | Representative patterns at different sizes of bounded domain.** Top row: Swarming; Bottom
532 row: Planktonic. The corresponding domain sizes and VOP values are marked as filled symbols. The
533 particle density is kept constant as the area of the simulated region increases.

534

535 **Figure S3**

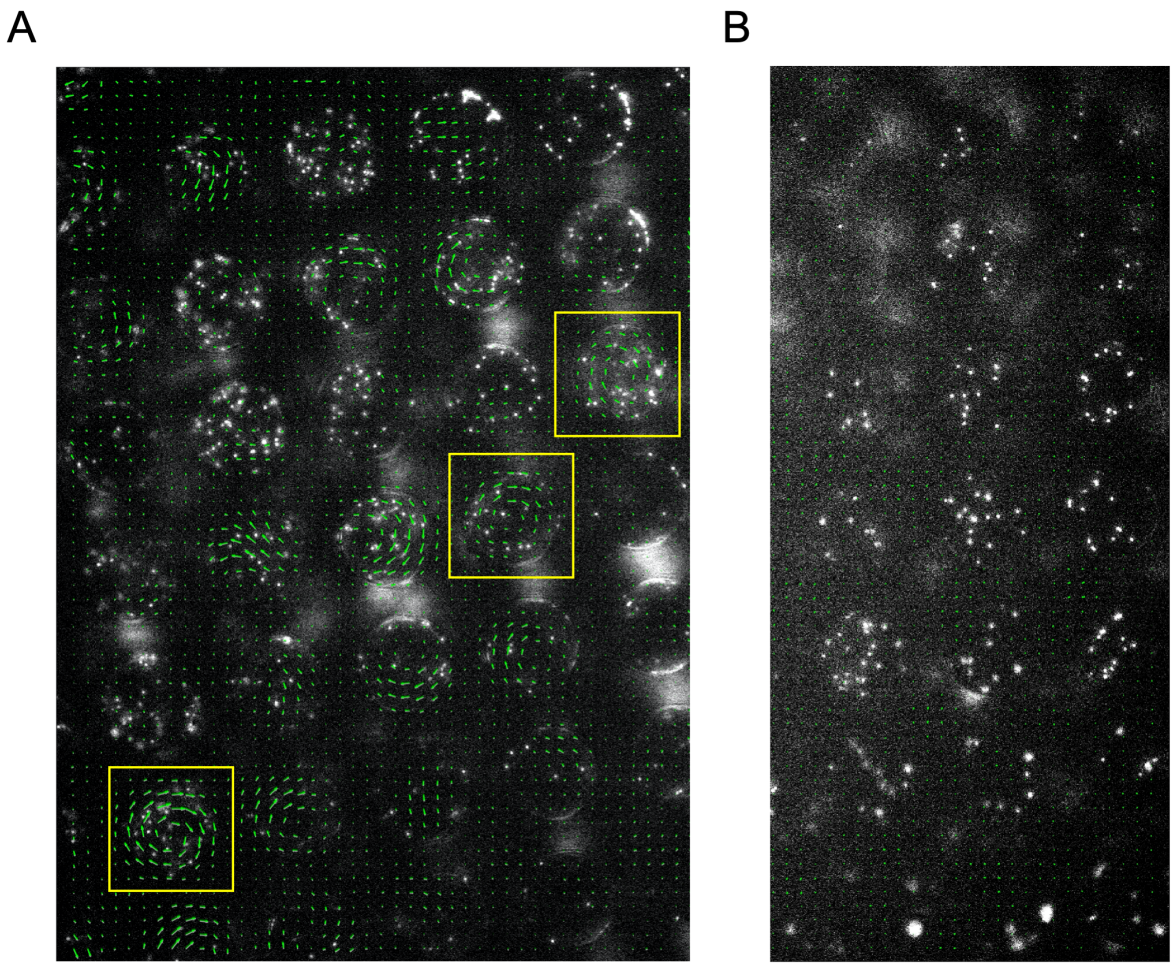


536

537 **Figure S3 | Fluorescent beads motion in microwells mounted on infected murine tissue.** PDMS chips
538 were coated with 0.5 μm fluorescent beads and mounted on SM3 inoculated colitic (A) or normal (B) mice
539 intestine tissue surfaces. Average velocity field was calculated by tracing the beads motion using PIV
540 toolkit. (A) On colitic tissue, wells with VOP > 0.7 were found and marked with yellow squares. We
541 conclude that, in these wells, the single swirl motion pattern of the beads was powered by the confined
542 swarming SM3. Since the tissue surface was not as smooth as on agar surface, the motion of the beads in
543 some wells did not form a complete vortex, yet jets indicating partial vortices can be seen. (B) On a normal
544 tissue lacking swarming bacteria, the average velocity of the beads in the wells due to random motion is
545 close to zero, thus the VOP is uniformly small. We could infer that the confined SM3 in these wells were
546 predominantly swimming rather than swarming.

## SI Methods

**Detecting bacterial motility on mouse intestine tissue using PDMS chips.** Six-week-old female C57BL/6 mice (Jackson Laboratories, Bar Harbor, ME; #000664) were administered 3%(w/v) DSS (Dextran Sulfate Sodium) (MPI; # 160110) in animal facility drinking water daily to induce acute colitis. After 9-12 days, when the mice weight loss reached 20%, mice were euthanized using isoflurane anesthesia and large intestines were harvested. For control, conventional six-week-old female C57BL/6 mice exposed to drinking water not containing DSS treatment were also sacrificed and the intestines were collected. This study was approved by the Institute of Animal Studies at the Albert Einstein College of Medicine, Inc (IACUC # 20160706 & 00001172). Intestine tissues were cut open, cleaned with 35%(v/v) ethanol, and rinsed with PBS twice. Tissues were spread on a 1% agar plate with inner side facing up, and overnight SM3 bacterial culture were inoculated on one end of the tissue. The agar plate was incubated under 37°C for 4.5 hours to allow SM3 bacteria to duplicate and move on the tissue surface. PDMS chips (d = 38 μm) were coated with 0.5 μm fluorescent beads (Dragon green; Bangs Laboratory, IN) and cut into strips to fit the size of the tissue. The PDMS strip was mounted and covered the tissue surface. Bead motion was observed under the fluorescent microscope (Olympus CKX41) with 20X objectives.

**Numerical simulations.** The dynamics of $N$ interacting active particles have been modeled in a 2-dimensional space using the overdamped Langevin-based equations, assuming that inertia is negligible in a low Reynolds number environment. The position $\boldsymbol{r}$ and orientation $\theta$ of particle $i$ are calculated using the following stochastic differential equations:

$$\partial_t \boldsymbol{r_i} = v_0 \widehat{p_\iota} - \sum_{j \neq i} k_{ex} r_{ji} \mathcal{H}(d_{ex} - r_{ji}) + \sqrt{2D_T}\xi_i \quad (1)$$

$$\partial_t \theta_i = \sum_{j \neq i} F_\theta(\boldsymbol{r_{ji}}, \widehat{p_\iota}, \widehat{p_j}) + \sqrt{2D_r}\zeta_i \quad (2)$$

Based on our experimental observations, bacterial velocity in the suspension is largely independent of the local cell density. Accordingly, the self-propulsion speed of particles is set to be a constant $v_0$ along the direction $\widehat{p_\iota} = [\cos(\theta_i), \sin(\theta_i)]$. The second term incorporates the central exclusion force term with a spring constant $k_{ex}$ which acts over the relative distance $r_{ji}$ with all the neighboring particles $j$. This exclusion force term applies only when $r_{ji}$ gets smaller than the

exclusion range $d_{ex}$ (represented as a Heaviside function H). The last term in Eq. (1) is the Brownian fluctuation term with the corresponding translation diffusivity $D_T$ and $\xi_i$ is the white noise with zero mean and correlation $\delta(t)$.

The temporal change in the orientation of each particles is influenced by two terms. The first term on the right-hand side of Eq. (2) includes all the binary interaction terms. The last term on the right-hand side of Eq. (2) is the contribution from the angular Brownian fluctuation with the rotational diffusion $D_r$ and a zero mean and delta-correlated stochastic white noise $\varsigma$. In the present study, we employ the pair-wise interaction model introduced previously[21,22], which successfully reproduces various macroscopic patterns reminiscent of bacterial suspensions. The pair-wise interaction term is based on a zonal model (Figure S4 below) which captures the alignment, anti-alignment and repulsion effects, and is formulated in the following form[21,22]:

$$F_\theta\left(\boldsymbol{r_{ji}}, \widehat{p_i}, \widehat{p_j}\right) = k_r\, \mathcal{H}\left(r_r - r_{ji}\right)\sin\left(\theta_i - \theta_{ji}\right) + \mu \sin\left(\theta_j - \theta_i\right) \quad (3)$$

$k_r$ is the magnitude of the constant repulsion interaction that applies over distance of $r_r$ around the particle (Fig. 1). The second term in Eq. (3) represents the alignment and anti-alignment effects, which operate over a range of $r_a$ and $r_{aa}$, respectively. The magnitude of the aligning interaction m is distance-dependent and is defined as [1, 2]:

$$\mu = \begin{cases} \mu^+\left(1 - (r_{ji}/r_a)^2\right) & 0 \le r_{ji} \le r_a \\ -\mu^- \dfrac{4(r_{ji} - r_a)(r_{aa} - r_{ji})}{(r_{aa} - r_a)^2} & r_a \le r_{ji} \le r_{aa} \end{cases} \quad (4)$$

where $m^+$ and $m^-$ are the strength of alignment and anti-alignment interactions, respectively.

We numerically integrate Eqs. (1) and (2) using the first order Euler scheme. Initially, the particles are randomly distributed with random orientations. The integration time step $\Delta t$ is selected sufficiently small to ensure both numerical stability and also independence of long-term statistics from $\Delta t$. The simulation time is set long enough to let the system reach a dynamic steady-state. The interaction of particles with the bounded circular domain is modeled via a reflective boundary condition.

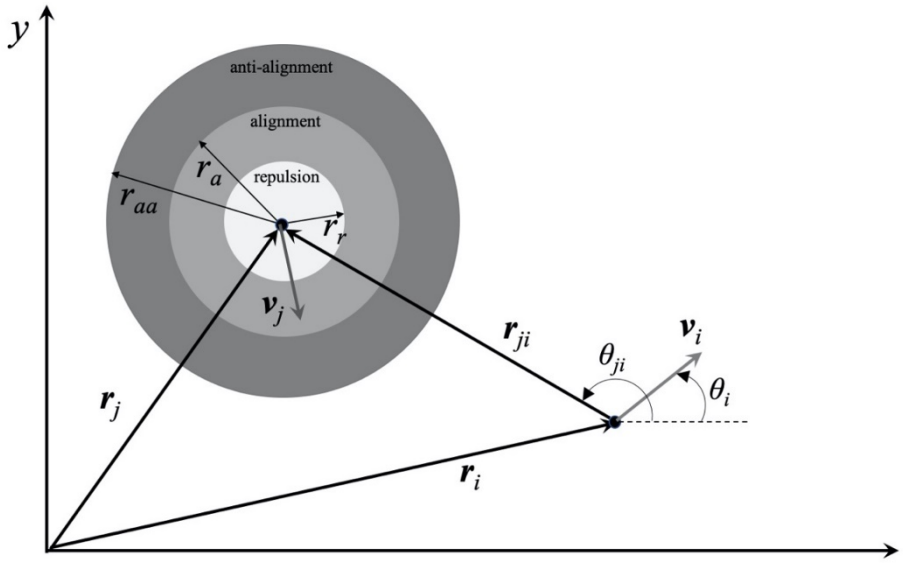


**Figure S4 | Schematic of the zonal pair-wise interaction model showing anti-alignment, alignment, and repulsion zones with the corresponding interaction radii $r_{aa}$, $r_a$ and $r_r$.**

In order to differentiate the Swarming and Planktonic cases, two different sets of interaction parameters have been used, which are summarized in Table 1. The values are unitless. In both systems, we set the exclusion parameters $k_{ex}$ and $d_{ex}$ to fixed values of 0.02 and 0.035, respectively. It is also assumed that particles only experience a rotational diffusion $D_r$ of 0.75. The simulations for both Swarming and Planktonic cases have been performed at two particle densities $r = N/A_{dom}$, where $N$ is the number of particles and $A$ is the area of the simulation domain. In the high density case, r = 4300 and in the diluted case, we set r = 235. In the diluted case, in order to further minimize the boundary effects, we replace the bounded domain with a periodic boundary.

| | | Swarming | Planktonic |
|---|---|---|---|
| **repulsion** | $k_r$ | 2 | 3 |
| | $r_r$ | 0.05 | 0.08 |
| **alignment** | $m^+$ | 0.5 | 0.2 |
| | $r_a$ | 0.2 | 0.2 |
| **Anti-alignment** | $m^-$ | 0.5 | 4.0 |
| | $r_{aa}$ | 0.25 | 0.25 |

**SI Methods Table 1 | Simulation parameters used for the Swarming and Planktonic cases**

## SI Movies

All videos play in real time, with the exception of Movie S5 & S6 which were taken in 20 fps but compressed in 30 fps.

**Movie S1: Confined swarming SM3 showing single swirl motion pattern.** Swarming SM3 was confined in 74 μm diameter PDMS wells.

**Movie S2: Confined concentrated planktonic SM3 showing turbulent motion pattern.** Swimming SM3 was confined in 74 μm diameter PDMS wells.

**Movie S3: Diluted swarming SM3 colony.** Swarming SM3 colony edge was diluted by adding a 50 μL water droplet. Clusters of bacteria cells formed rafts.

**Movie S4: Diluted swimming SM3 suspension.** Concentrated planktonic SM3 was diluted by adding a 50 μL water droplet. Bacteria cells were observed to swim independently without clustering.

**Movie S5: Fluorescent beads motion on DSS induced colitic mouse intestine tissue.** The unidirectional rotation motion in 38 μm diameter wells indicates swarming SM3 on the tissue surface.

**Movie S6: Fluorescent beads motion on normal mouse intestine tissue.** The random motion in 38 μm diameter wells indicates planktonic SM3 on the normal mice tissue surface.

**Movie S7: Numerical simulations of circularly confined SM3.** Swarming SM3 (left) and concentrated planktonic SM3 (right) were simulated in the well size of 0.48. The video shows the representative confined motion pattern. Arrows indicate the moving direction of the particles.

**Movie S8: Numerical simulations of SM3 cells in open space.** Diluted swarming SM3 (left) and planktonic SM3 (right) were simulated without confinement with a periodic boundary condition. Cell density in both cases are $\rho = 235$, and the arrows indicate the moving directions of the particles.